Available online at www.sciencedirect.com
SCIENCE DIRECT®
Journal of Solid State Chemistry 178 (2005) 613–620
JOURNAL OF SOLID STATE CHEMISTRY
www.elsevier.com/locate/jssc

The effects of the spinodal microstructure on the electrical properties of TiO_2–SnO_2 ceramics

Wanwilai Chaisan[a,*], Rattikorn Yimnirun[a], Supon Ananta[a], David P. Cann[b]

[a]*Department of Physics, Faculty of Science, Chiang Mai University, Chiang Mai, Thailand*
[b]*Materials Science and Engineering Department, Iowa State University, Ames, IA, USA*

Received 18 October 2004; received in revised form 29 November 2004; accepted 30 November 2004

Abstract

The electrical properties of ceramics within the TiO_2–SnO_2 system which exhibit spinodal decomposition were investigated under different annealing conditions. Changes in the lattice parameter and the phase evolution of the spinodal decomposition, measured in terms of the volume fraction transformed $X(t)$, were examined as a function of annealing time using X-ray diffraction. The room temperature dielectric properties were measured and compared to dielectric mixing rules. Doping with pentavalent Nb was found to slow the decomposition kinetics and a high permittivity ($\varepsilon_r > 1000$) was induced. The origin of the high permittivity is linked to the formation of an electrically heterogeneous structure which is derived from the spinodal microstructure. Lastly, it was observed that Nb-doped TiO_2–SnO_2 ceramics exhibited non-linear current–voltage behavior which can be attributed to the negative temperature coefficient of resistance effect.

Keywords: Electrical properties; Spinodal decomposition; Titania; Tin oxide; Maxwell–Wagner polarization

1. Introduction

Spinodal decomposition is a mechanism for phase separation which leads to a characteristic modulated structure which can be exploited to control the microstructure at the nanometer scale. Numerous metal oxide and non-oxide systems, such as Al_2O_3–Cr_2O_3 [1,2], $CoFe_2O_4$–Co_3O_4 [3,4] and AlN–SiC [5,6], are known to decompose through spinodal mechanisms. However, only a few of these systems have had their dielectric properties characterized. The ZrO_2–SiO_2 system was analyzed by Kim and Mclntyre [7] for high permittivity gate dielectric applications. In the $LiTaO_3$–SiO_2 glass system [8], the dielectric properties were examined during the phase transition. Their results showed anomalous dielectric peaks on heating which was explained on the basis of structural relaxations and multiple phases arising from the supercooled phase and spinodal decomposition. Moreover, spinodal decomposition occurs in $Ba_{2-x}Sr_xTiO_4$ ceramics [9] and the dielectric data has been shown to vary with composition.

Spinodal decomposition was first noted in the SnO_2–TiO_2 system by Padurow [10]. The two constituent oxides SnO_2 and TiO_2 both form the rutile structure ($A^{VI}X_2^{III}$) with complete solid solubility above 1450 °C. At the approximate composition $Sn_{0.5}Ti_{0.5}O_2$, below 1450 °C spinodal decomposition results in a modulated structure consisting of a SnO_2-rich phase and a TiO_2-rich phase with compositional modulation length of $\lambda \approx 10-100$ nm. Due to the tetragonal structure of rutile, the spinodal structure exhibits strong anisotropic features.

Spinodal systems commonly involve two phases with similar crystal structures and similar materials properties. Therefore, the properties of the spinodal structure

*Corresponding author. Department of Material Science and Engineering, Electroceramics Research Group, Iowa State University, Room 2220, Hoover Hall, Ames, IA 50011, USA. Fax: +515 294 5444.
E-mail address: wanwilai@iastate.edu (W. Chaisan).

0022-4596/$ - see front matter © 2005 Elsevier Inc. All rights reserved.
doi:10.1016/j.jssc.2004.11.030

Table 1
Summary of structural, dielectric and optical properties of TiO_2 and SnO_2

Property	TiO_2	SnO_2
Lattice parameters	$a = 4.737$ Å $c = 3.186$ Å	$a = 4.5931$ Å $C = 2.9586$ Å
Static permittivity, ε_r	114	12.6
Refractive index, n	2.71	1.98

derived from these systems show no extraordinary features. Among all spinodal systems the SnO_2–TiO_2 is unique in that while both phases are isostructural, the two phases have very different chemical, electronic, and optical properties. Table 1 summarizes the contrasts between the optical and dielectric properties of the two phases.

The coordination number of tin and titanium are the same, and the cation to anion radius ratios are nearly identical, being 0.51 and 0.49, respectively. Since Sn and Ti are isovalent, the addition of SnO_2 does not influence the defect chemistry of TiO_2. However, SnO_2 has a rutile tetragonal crystal structure with no anatase analog and thus can be expected to stabilize the rutile phase in TiO_2. Therefore, there has been a considerable amount of work focused on phase transformations within the TiO_2–SnO_2 binary system. Moreover, great attention has been paid to the TiO_2–SnO_2 system for applications such as gas sensors because this system seems to combine the positive features of both materials.

Since Cahn's work [11] on the thermodynamics and kinetics of spinodal decomposition in metallic binary systems, there have been numerous studies about spinodal decomposition in a broad range of materials systems. The TiO_2–SnO_2 system has been examined in depth with detailed studies about the phase separation mechanism and attempts to predict the phase diagram of this system.

Stubican and Schultz [12,13] were the first to analyze the spinodal decomposition in the TiO_2–SnO_2 system. They fired samples at $1750 \pm 10\,^{\circ}C$ for 20–30 min and quenched in water. After the formation of crystalline solutions, specimens were annealed at various temperatures within the miscibility gap. X-ray diffraction (XRD) patterns and electron micrographs were used for determining the phase evolution in this system. From their results, they found that the decomposition proceeded as follows: crystalline solid solution → intermediate modulated phase (coherent) → equilibrium phases (incoherent). Moreover, they used theoretical calculations to find the elastic free energy/unit volume which caused the compositional fluctuations in the spinodal process in a tetragonal system. They found that the theoretical prediction and the experimental results for the TiO_2–SnO_2 system agreed well.

In other work, Park et al. [14] used large angle X-ray diffraction (LAXD), small-angle X-ray scattering (SAXS), transmission electron microscopy (TEM) and electron diffraction to study the decomposition of TiO_2–SnO_2 and characterized the spinodal structure of this system. The results of their work indicated that compositions within the spinodal region decompose by a continuous and spontaneous process, whereas compositions outside the spinodal decompose by a discontinuous and non-spontaneous process. Furthermore, Park et al. [15] reevaluated the subsolidus phase equilibria in TiO_2–SnO_2 system and they found that the miscibility dome was nearly symmetric. The critical composition and critical temperature were 47 mol% and 1430 °C, respectively.

The molten-salt method was used for determining the low-temperature region of the TiO_2–SnO_2 phase diagram down to a temperature of 400 °C. A comparison with the phase diagram determined from conventional solid-state-annealing methods revealed that the phase diagrams are similar above 1100 °C [16]. However, equilibrium compositions are closer to the end members below 1100 °C. This is attributed to sluggish solid-state kinetics at low temperature.

Virkar et al. [17–19] examined the effects of aliovalent dopants on the spinodal decomposition kinetics in the TiO_2–SnO_2 system. Their work demonstrated that aliovalent dopants not only alter the kinetics but also affect the resulting precipitate morphology. Moreover, they applied Raman spectroscopy to study the phase transformation in $Ti_{0.65}Sn_{0.35}O_2$ [20] and found that Raman shifts were in good agreement with data from X-ray studies. Recently, Hirata et al. [21] studied the effect of concentration on optical phonons in the TiO_2–SnO_2 system by using Raman scattering and Fourier-transform infrared spectroscopy. Shi et al. [22] presented a new method to synthesize ultra fine SnO_2–TiO_2 semiconductor particles and discussed the related morphology and properties of this system. Edelman et al. [23] used reactive ion sputtered (RIS) and molecular beam techniques to create SnO_2–TiO_2 films. In situ TEM, XRD, SEM, Raman and IR-spectroscopy were used to analyze the structural transformations in these films.

All of the previous work has been concentrated on discussing the spinodal decomposition and phase transformations in the TiO_2–SnO_2 system with some complementary characterization of the optical properties. However there is no information pertaining to the dielectric and electrical properties of this system. In this work, the electrical properties of $0.5TiO_2$–$0.5SnO_2$ ceramics prepared via solid-state synthesis are presented. The present work aims to provide a comprehensive study on the dielectric and electrical properties relationships in the spinodal binary system of TiO_2–SnO_2.

2. Experimental procedure

The $0.5TiO_2$–$0.5SnO_2$ powder was prepared via solid-state reaction from reagent grade oxides of anatase TiO_2 (Fisher Chemicals 99.9%) and rutile SnO_2 (Alfa Aesar 99.9%). After weighing, the mixture of TiO_2 and SnO_2 powders were homogeneously vibratory-milled with zirconia media in ethanol for 6 h. The well-mixed powder was calcined at 1100 °C for 6 h with a heating/cooling rate 5 °C/min in an alumina crucible. After drying and grinding, the powder was then mixed with approximately 5 wt% organic binder and 12.5 mm diameter pellets were prepared by cold uniaxial pressing. The $0.5TiO_2$–$0.5SnO_2$ pellets were sintered at 1450 °C for 24 h at a heating rate of 5 °C/min followed by air quenching. Finally, the $0.5TiO_2$–$0.5SnO_2$ ceramics were annealed at 1000 °C for various times (1,4,10 and 48 h) with a heating rate of 10 °C/min and quenched in air after the specified time, in order to investigate the phase transformation and phase decomposition kinetics. The donor dopant Nb_2O_5 was used to modify the conductivity and the phase decomposition kinetics. The Nb-doped samples (0.36 and 1.0 Nb mol%) were formulated by employing a similar procedure as described above and were annealed at 1000 °C for 1, 10 and 100 h. These doping levels were chosen because Drobeck et al. have shown that these dopant concentrations will yield rates of phase evolution during spinodal decomposition [24].

To obtain a uniform quench rate and to minimize the effects of reduction at high temperatures, the thickness of the specimens was limited to less than 1 mm. In addition, to minimize surface effects such as SnO_2 volatilization the surface of the pellets was ground to a final thickness of approximately 0.5 mm.

The calcined powder and sintered pellets were examined by XRD using CuK_α radiation to identify the phase evolution. Room temperature dielectric properties were measured as a function of frequency from 100 Hz to 100 kHz. Relative permittivity (ε_r) was calculated using the geometric area and thickness of the discs. Current–voltage measurements were carried out at room temperature using a source measure unit (Keithley 237). All electrical measurements were carried out using silver electrodes.

Samples were prepared for TEM examination using conventional mechanical dimpling followed by argon ion milling. A Phillips CM30 TEM operated at 300 kV was used to obtain the microstructural images.

3. Results and discussions

After mixing the two precursors together, anatase TiO_2 and rutile SnO_2, the calcined $0.5TiO_2$–$0.5SnO_2$ powder was analyzed by XRD. To a first approximation, it was observed that the powder calcined at 1100 °C consisted of equal amounts of the mixed phases of rutile-TiO_2 and rutile-SnO_2. The XRD data from TiO_2 indicates that after calcination at 1100 °C the anatase structure converted to the rutile structure. This is in agreement with the results of other work [25]. After sintering the $0.5TiO_2$–$0.5SnO_2$ ceramics at 1450 °C for 24 h and quenching in air, the XRD pattern of this ceramic displayed a single-phase solid solution (♦) based on the rutile structure (Fig. 1).

XRD patterns of $0.5TiO_2$–$0.5SnO_2$ ceramic samples annealed at 1000 °C for various times are shown in Fig. 1. The data show that prior to annealing, the quenched ceramic exhibited a crystalline solid solution (♦) with well-defined peaks. The (hkl) indices for each peak are identified in the figure. After annealing at 1000 °C, the (011) peak at $2\theta \approx 35.45^\circ$ and the (211) peak at $2\theta \approx 53.55^\circ$ both indicate splitting. This is consistent with the spinodal decomposition reaction:

$$(Sn_{0.5}Ti_{0.5}O_2)_{SS} \rightarrow SnO_2 + TiO_2. \quad (1)$$

It must be noted that the SnO_2 and TiO_2 phases in Eq. (1) are not pure. Rather the phase diagram predicts Sn- and Ti-rich phases, both with the rutile structure.

Fig. 2 presents the (011) peak of the annealed samples which highlights the splitting. After annealing for 1 h, the intensity of the solid solution phase decreased and a distinct peak appeared at higher *d*-spacings which indicates that the SnO_2 phase had formed. With increased annealed time, the TiO_2 peak was observed at lower *d*-spacings and the (011) solid solution peak gradually disappeared. After annealing for 48 h, it is seen that the SnO_2 and TiO_2 phases had completely

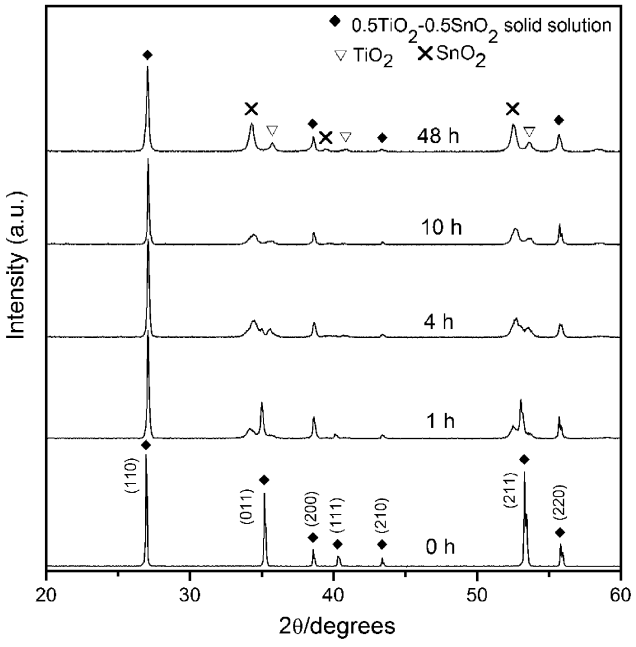

Fig. 1. XRD patterns of the annealed $0.5TiO_2$–$0.5SnO_2$ ceramics at 1000 °C for various times.

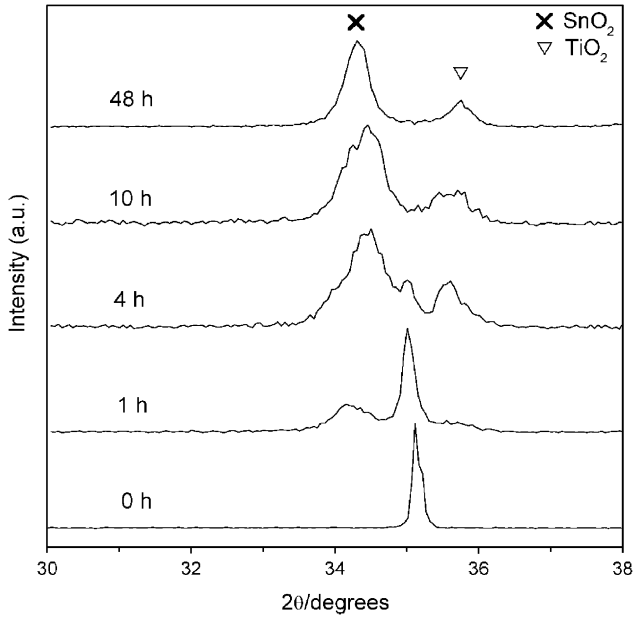

Fig. 2. XRD patterns show the phase decomposition of $0.5TiO_2$–$0.5SnO_2$ ceramics as a function of annealing time.

separated and moreover the original solid solution (011) peak completely disappeared. The XRD results of this work agree well with other workers which studied the phase decomposition of this system by using both XRD and TEM [12,14,19].

The lattice parameters a and c were determined by using a non-linear least-squares method [26]. Figs. 3(a) and (b) show a- and c-parameters as a function of annealing times, respectively. As shown in Fig. 3(a), the value of the a parameter increased significantly after annealing for 1 h. This lattice expansion is likely due to re-oxidation of the samples after reduction during the high-temperature quenching process [27]. At longer annealing times, the a- and c-parameters for SnO_2 and TiO_2 split due to the decomposition reaction.

The volume fraction transformed, $X(t)$, was estimated by determining the integrated intensities of the (011) solid solution peak and the SnO_2 and TiO_2 peaks. Fig. 4 shows the relationship between the volume fraction transformed as the function of the annealing time. From this graph, it was found that the phase transformation of $0.5TiO_2$–$0.5SnO_2$ obeys with the theory of transformations [28] and agrees well with the previous study [18].

Table 2 presents the relative permittivity (ε_r) versus frequency at room temperature of $0.5TiO_2$–$0.5SnO_2$ ceramics annealed at 1000 °C for various times. It can be seen that the ε_r of all samples remained largely unchanged with increased annealing time. From a simple logarithmic mixing rule and using the data from Table 1 (neglecting porosity) the composite

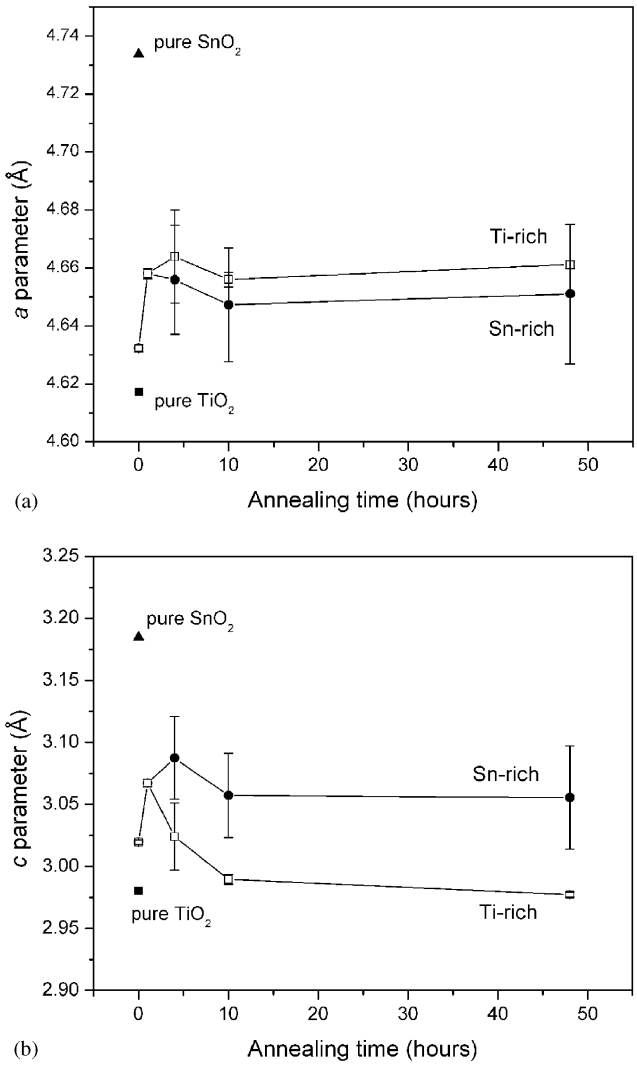

Fig. 3. (a) The a lattice parameter and (b) c lattice parameter as a function of annealing time in the $0.5TiO_2$–$0.5SnO_2$ ceramics.

Table 2
Dielectric constant (ε_r) and dielectric loss ($\tan\delta$) at 10 kHz for $0.5TiO_2$–$0.5SnO_2$ ceramics annealed at 1000 °C for various times

Annealing time (h)	Dielectric constant (ε_r)	Dielectric loss ($\tan\delta$)
0	42.7±0.21	0.0012±0.0010
1	44.0±0.38	0.0011±0.0017
4	44.5±0.71	0.0005±0.0002
10	41.7±0.29	0.0010±0.0008
48	45.6±1.24	0.0019±0.0014

permittivity can be written as:

$$\ln \varepsilon_r = V_{TiO_2} \ln \varepsilon_{r,TiO_2} + V_{SnO_2} \ln \varepsilon_{r,SnO_2}, \quad (2)$$

where ε_r is the permittivity and V is the volume fraction. The permittivity for the $0.5TiO_2$–$0.5SnO_2$ solid solution should be approximately 40.8. The variations in

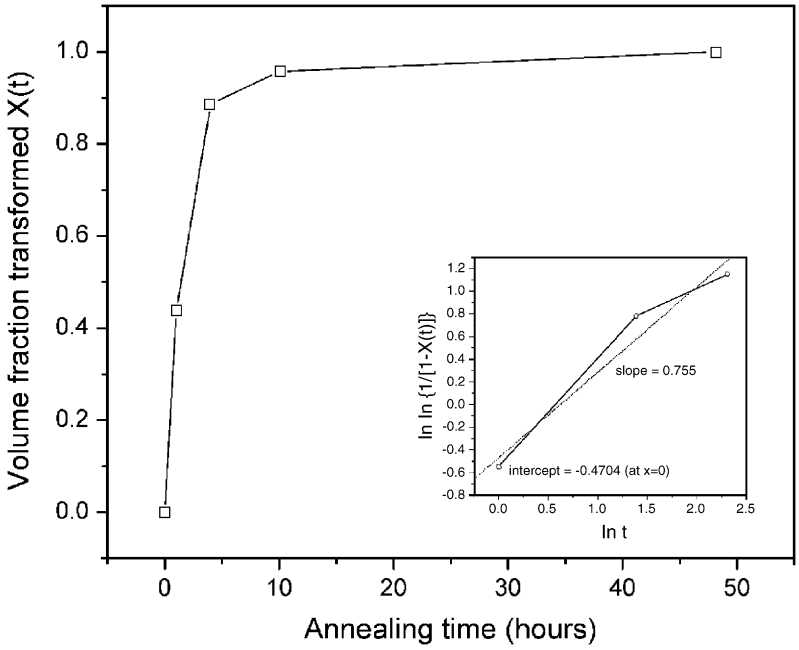

Fig. 4. Plot of volume fraction transformed, $X(t)$, of $0.5TiO_2$–$0.5SnO_2$ ceramics as a function of annealing time.

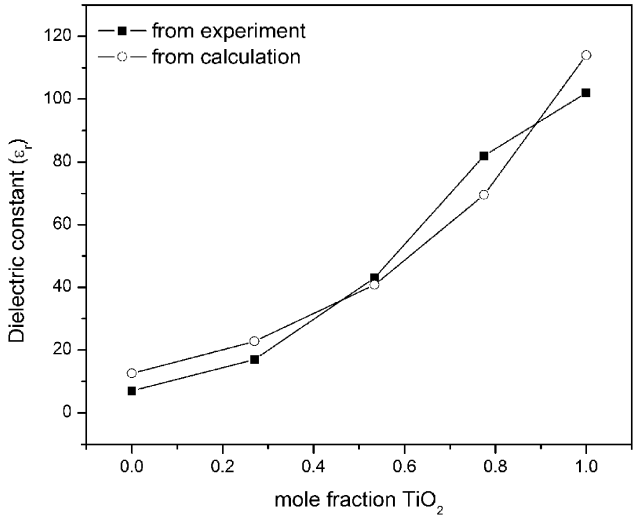

Fig. 5. Dielectric constant (ε_r) of TiO_2–SnO_2 system.

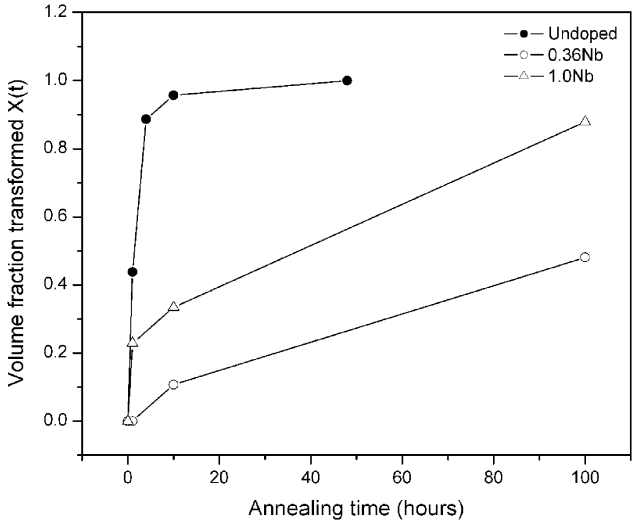

Fig. 6. Plot of volume fraction transformed, $X(t)$, of undoped and doped samples of $(Ti_{0.5}Sn_{0.5})O_2$ as a function of annealing time.

permittivity values can be attributed to the observed porosity in these compositions. The highest permittivity values were recorded for ceramics annealed at 1000 °C for 48 h. All of the samples exhibited low dielectric loss characteristics ($\tan\delta \ll 1\%$). Unfortunately there was a considerable error in the loss measurements due to the fact that the small size of the samples (required to obtain a uniform quench rate) led to low capacitance values thus making the loss measurements inherently problematic.

Fig. 5 shows the dielectric properties of ceramics across the TiO_2–SnO_2 binary system at 10 kHz compared to the calculated values using Eq. (2). In general the measured values are comparable to the calculated values except for the effects of porosity observed in the Sn-rich compositions.

Doping with pentavalent Nb at levels of 0.36 and 1.0 mol% had the effect of slowing down the decomposition reaction as shown in Fig. 6. In addition, Nb-doping was found to dramatically increase the permittivity to values above 1000 (Figs. 7 and 8). The dielectric loss data reveals a peak in $\tan\delta$ near 1 MHz which is indicative of a dielectric relaxation due to space charge polarization. As the frequency increased, the

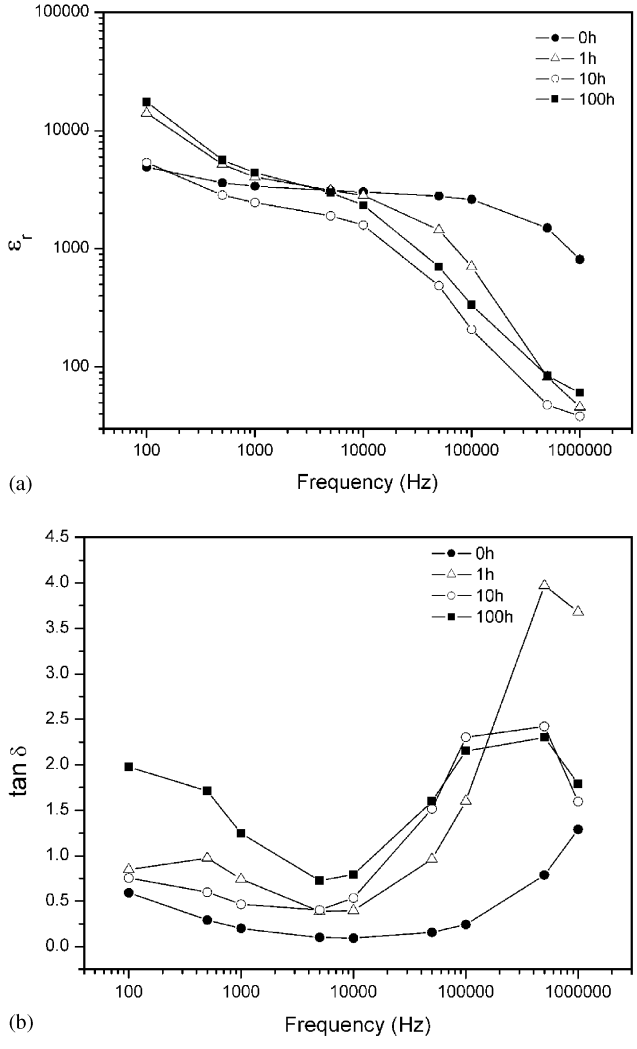

Fig. 7. (a) Dielectric constant (ε_r) and (b) dielectric loss ($\tan\delta$) as a function of frequency of $(Ti_{0.5}/Sn_{0.5})O_2 + 0.36$ mol% Nb ceramics.

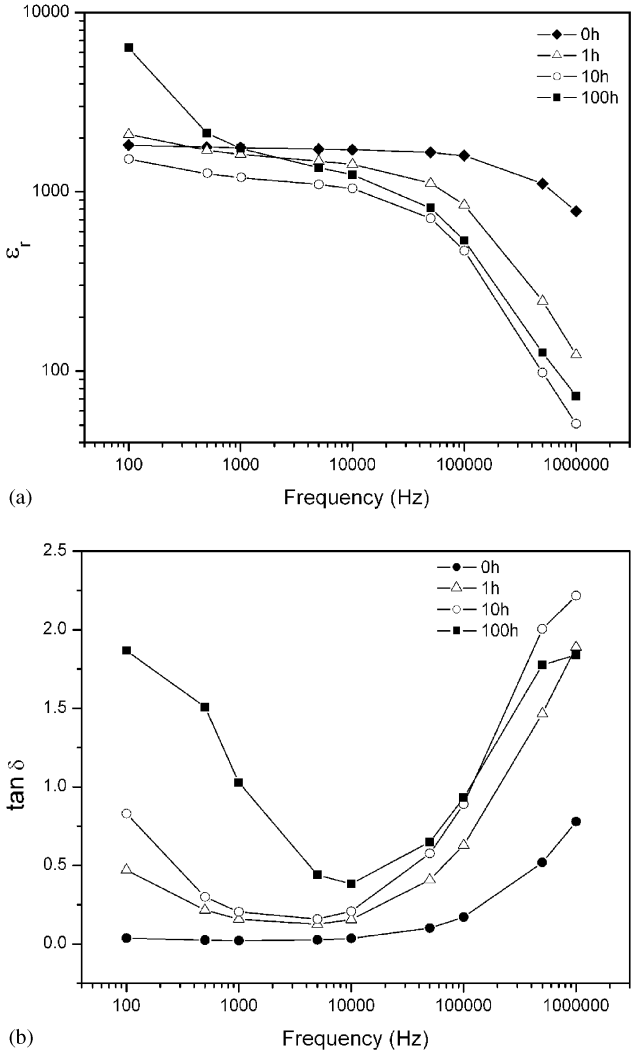

Fig. 8. (a) Dielectric constant (ε_r) and (b) dielectric loss ($\tan\delta$) as a function of frequency of $(Ti_{0.5}/Sn_{0.5})O_2 + 1.0$ mol% Nb ceramics.

permittivity decreased towards a value close to the permittivity of undoped $0.5TiO_2$–$0.5SnO_2$ ($\varepsilon_r \approx 40$). Overall, this dielectric behavior is likely due to an inhomogeneous conductivity arising from a non-uniform distribution of the Nb dopant. It is known that Nb exhibits a large degree of solid solubility in TiO_2 with a maximum of over 10 mol% at the processing temperatures in this study [29]. While there are no published phase diagrams of the SnO_2–Nb_2O_5 system, the larger ionic radii mismatch between Nb^{5+} and Sn^{4+} is likely to result in a lower solubility. Assuming that electronic compensation is dominant at high temperatures, the Nb-doping should result in an enhanced conductivity in the TiO_2-phase [24].

The Maxwell–Wagner polarization model describes the dielectric response of a two phase structure in terms of a simple equivalent circuit consisting of two parallel RC elements in series (Fig. 9) [30,31]. The net

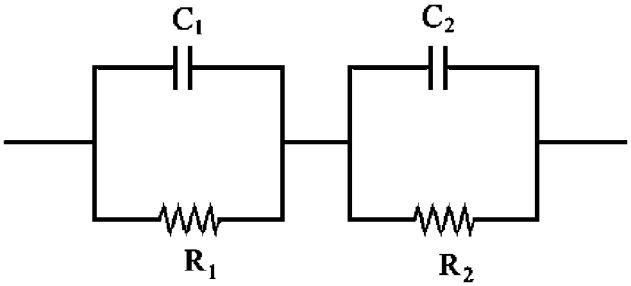

Fig. 9. Maxwell–Wagner circuit.

permittivity can thus be described via:

$$\varepsilon(\omega) = \frac{\varepsilon_s + \varepsilon_\infty \tau_\varepsilon^2 \omega^2}{1 + \tau_\varepsilon^2 \omega^2}, \quad (3)$$

where ε_s is the static permittivity, ε_∞ is the high-frequency permittivity (for $Ti_{0.5}Sn_{0.5}O_2$, $\varepsilon_\infty \approx 40$), ω is

the angular frequency ($\omega = 2\pi f$), and τ_ε is the relaxation time (defined from the frequency at which ε'' is maximum) which is given by

$$\tau_\varepsilon = \varepsilon_0 \frac{\varepsilon_1 d_2 + \varepsilon_2 d_1}{\sigma_1 d_2 + \sigma_2 d_1}. \quad (4)$$

The ε, σ, and d parameters correspond to the permittivity, conductivity, and thickness of the two phases, respectively. Space charge polarization in polycrystalline oxides is often related to heterogeneities associated with the grain and grain boundary structure. However, in the TiO_2–SnO_2 system the grain size remained constant for all processing conditions and therefore it is likely that the polarization is related to the lamellar structure associated with the spinodal decomposition. Fig. 10 presents a TEM image of the lamellar structure of an undoped $Ti_{0.5}Sn_{0.5}O_2$ ceramic which was annealed at 1000 °C for 48 h. The structure shows alternating layers of SnO_2 and TiO_2 lamellae at a thickness of approximately 26 nm.

Inspection of the data in Figs. 7 and 8 show that the permittivity tends to decrease with increased annealing time. In addition as the annealing time increased it was observed that the $\tan\delta$ peak shifted to lower frequencies. From Eq. (4) there are many factors that could contribute to a shift in τ_ε. It is certainly the case that as the annealing time increased, the spinodal microstructure evolved with an increase in lamellae size. However, the dramatic increase in dielectric loss at low frequencies suggests that an increase in conductivity is responsible for the shift.

Fig. 11 presents the temperature dependence of the permittivity of the 1.0 mol% Nb-doped sample. In the vicinity of room temperature, the permittivity from 1 to 100 kHz is remarkably stable. For example, the permittivity at 10 kHz varies less than 0.3% from 0 to 100 °C. Table 3 presents the room temperature data at 10 kHz and it is apparent that the unannealed 1.0% Nb-doped material maintains a high permittivity of 1700 and a relatively low loss of 0.03.

Fig. 10. TEM image of $(Ti_{0.5}/Sn_{0.5})O_2$ ceramics annealed for 48 h.

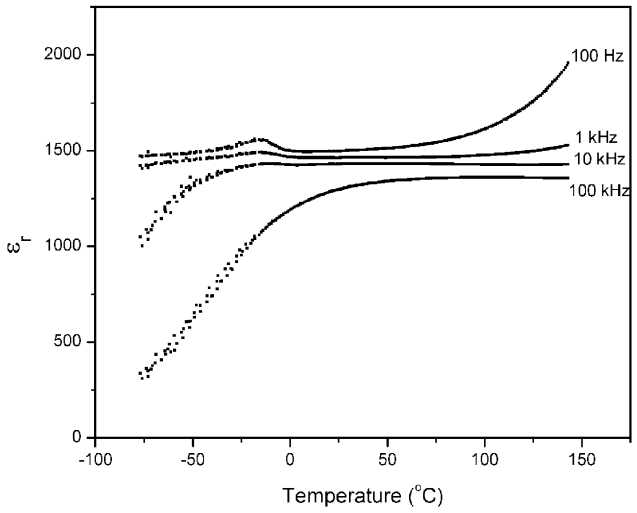

Fig. 11. Dielectric constant (ε_r) versus temperature of the 1.0 mol% Nb-doped sample.

Table 3
Dielectric constant (ε_r) and dielectric loss ($\tan\delta$) at 10 kHz for Nb-doped samples annealed at 1000 °C for various times

Annealing time (h)	0.36 mol% Nb		1.0 mol% Nb	
	Dielectric constant (ε_r)	Dielectric loss ($\tan\delta$)	Dielectric constant (ε_r)	Dielectric loss ($\tan\delta$)
0	3020	0.09	1720	0.03
1	2830	0.40	1430	0.15
10	1590	0.53	1040	0.21
100	2340	0.79	1250	0.38

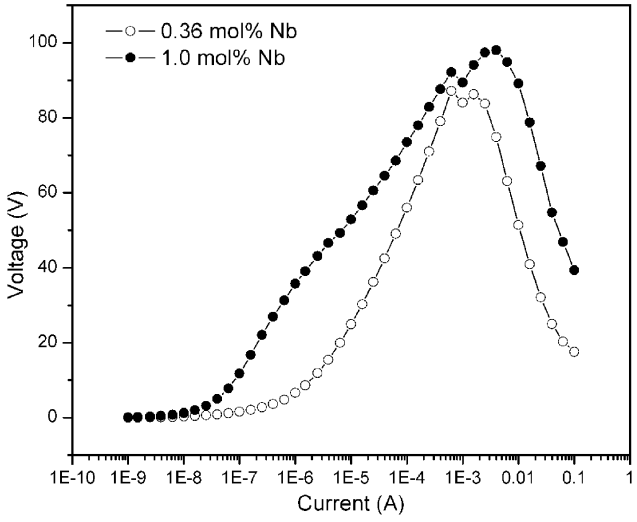

Fig. 12. *I–V* graphs of $(Ti_{0.5}/Sn_{0.5})O_2$ ceramics doped with Nb.

The current–voltage behavior of the Nb-doped ceramics is shown in Fig. 12. Both samples exhibited a non-linear I–V behavior with a voltage maxima near 1 mA. This behavior is commonly associated with heating and is indicative of a negative temperature coefficient (NTC) of resistivity effect.

4. Conclusions

In this work, the effects of the spinodal decomposition on the electrical properties in the SnO_2–TiO_2 binary system were examined. It was demonstrated that the spinodal structure could be controlled through annealing and through cation doping. It was observed that permittivity of undoped SnO_2–TiO_2 ceramics closely followed a logarithmic mixing rule. Doping with Nb was found to induce permittivities in excess of 1000 due to space charge effects that arose from a heterogeneous conductivity. Finally, Nb-doped compositions also were found to exhibit the NTC effect in current–voltage measurements.

Acknowledgments

The authors would like to thank Dr. Xiaoli Tan and He Hui, Materials Science and Engineering, ISU, for contributing the TEM micrograph to this study. This work was supported by the Thailand Research Fund (TRF), Graduate School of Chiang Mai University and the Ministry of University Affairs.

References

[1] A.H. Schultz, V.S. Stubican, J. Am. Ceram. Soc. 53 (1970) 613–616.
[2] V.S. Stubican, A.H. Schultz, W.R. Bitler, Philos. Mag. 22 (1972) 993–1001.
[3] M. Takahashi, J.R.C. Guimaraes, M.E. Fine, J. Am. Ceram. Soc. 54 (1971) 291–295.
[4] M. Takahashi, M.E. Fine, J. Am. Ceram. Soc. 53 (1970) 633–634.
[5] J. Chen, Q. Tian, A.V. Virkar, J. Am. Ceram. Soc. 75 (1992) 809–821.
[6] M. Miura, T. Yogo, S. Hirano, J. Mater. Sci. 28 (1993) 3859–3865.
[7] H. Kim, P.C. Mclntyre, J. Appl. Phys. 92 (2002) 5094–5102.
[8] S.J. Kim, J.E. Kim, Y.S. Yang, Ferroelectrics 272 (2002) 321–326.
[9] V. Shanker, T. Ahmad, A.K. Ganguli, Bull. Mater. Sci. 27 (2004) 421–427.
[10] N.N. Padurow, Naturwissenschaften 43 (1956) 395.
[11] J.W. Cahn, J. Chem. Phys. 42 (1965) 93–99.
[12] V.S. Stubican, A.H. Schultz, J. Am. Ceram. Soc. 51 (1968) 290–291.
[13] V.S. Stubican, A.H. Schultz, J. Am. Ceram. Soc. 53 (1970) 211–214.
[14] M. Park, T.E. Mitchell, A.H. Heuer, J. Mater. Sci. 11 (1976) 1227–1238.
[15] M. Park, T.E. Mitchell, A.H. Heuer, J. Am. Ceram. Soc. 58 (1975) 43–47.
[16] H.P. Naidu, A.V. Virkar, J. Am. Ceram. Soc. 81 (1998) 2176–2180.
[17] A.V. Virkar, M.R. Plichta, J. Am. Ceram. Soc. 66 (1983) 451–456.
[18] T.C. Yuan, A.V. Virkar, J. Am. Ceram. Soc. 69 (1986) C310–C312.
[19] T.C. Yuan, A.V. Virkar, J. Am. Ceram. Soc. 71 (1988) 12–21.
[20] R.M. Cohen, D. Drobeck, A.V. Virkar, J. Am. Ceram. Soc. 71 (1988) C401–C403.
[21] T. Hirata, K. Ishioka, M. Kitajima, H. Doi, Phys. Rev. B 53 (1996) 8442–8448.
[22] L. Shi, C. Li, H. Gu, D. Fang, Mater. Chem. Phys. 62 (2000) 62–67.
[23] F. Edelman, H. Hahn, S. Seifried, C. Alof, H. Hoche, A. Balogh, P. Werner, K. Zakrzewska, M. Radecka, P. Pasierb, A. Chack, V. Mikhelashvili, G. Eisenstein, Mater. Sci. Eng. B 69–70 (2000) 386–391.
[24] D.L. Drobeck, A.V. Virkar, R.M. Cohen, J. Phys. Chem. Sol. 51 (1990) 977–988.
[25] W.Y. Wang, D.F. Zhang, T. Xu, X.F. Li, T. Zhou, X.L. Chen, Mater. Res. Bull. 37 (2002) 1197–1206.
[26] B.D. Cullity, Elements of X-ray Diffraction, Addison-Wesley Publishing Company, Inc., Reading, MA (Wokingnam, UK), 1978 (p. 32).
[27] M.E. Straumanis, T. Ejima, W.J. James, Acta Crystallogr. 14 (1961) 493–497.
[28] J.W. Christian, The Theory of Transformations in Metals and Alloys: Part I, Pergamon Press, Oxford, 2002 (p. 16).
[29] R.S. Roth, Prog. Solid State Chem. 13 (1980) 159–192.
[30] L.M. Levinson, H.R. Philipp, J. Appl. Phys. 49 (1978) 6142–6146.
[31] J. Volger, Dielectric properties of solid in relation to imperfections, Wiley, New York, 1960 (p. 207).